Table VII. Vibrational Frequencies in Unsaturated Rings[a]

approximate description	freq, cm^{-1} X = C	X = Si	sym-metry
HCCH out-of-plane	782 (569)	823	b_1
HCC scis	1012 (905)	1093	a_1
HCCH twist	1035 (815)	1107	a_2
XH_2 twist	1125 (996)	623	a_2
XH_2 wag	1186 (1011)	707	b_2
XH_2 rock	1191 (1088)	652	b_1
HCCH wag	1216 (1043)	1268	b_2
XH_2 scis	1664 (1483)	1038	a_1
XH_2 sym str	3255 (2909)	2323	a_1
XH_2 antisym str	3332 (2995)	2314	b_1
=CH antisym str	3455 (3116)	3390	b_2
=CH sym str	3513 (3152)	3423	a_1

[a] Experimental frequencies given in parentheses for cyclopropane (see ref 17).

positive X-C $p\pi$-$p\pi$ overlap population.[14] In contrast, the ring deformation frequency is much "looser" in silacyclopropene, indicating that the effect of a small apex angle is less in this molecule.

Finally, both reactions 2 and 3 predict the strain in the two silicon rings to be very similar. This is particularly true for the 6-31G* calculations. Thus, introduciton of a C=C bond into cyclopropane has a much greater destabilizing effect than in silacyclopropane.

The vibrational frequencies (determined by using 3-21G) for the normal modes not involving ring motions are listed in Tables VI and VII for the saturated and unsaturated rings, respectively.[15] The experimental[16] frequencies for cyclopropane and cyclopropene are also given. Most of the trends are correctly reproduced, and the magnitudes are typically in error by about 10% for cyclopropane and 15-20% for cyclopropene. The one cyclopropane frequency seriously in error is the nondegenerate CH_2 scissor motion. Interestingly, the corresponding frequency in cyclopropene is closer to the experimental value. Not surprisingly, the frequencies for motions involving silicon are typically considerably smaller than the corresponding carbon frequencies. This is particularly apparent for the XH stretching motions which are predicted to differ by as much as 1000 cm^{-1}. This appears to be a reasonable estimate in view of typical experimental[16] SiH stretching frequencies.

Acknowledgment. This work was supported in part by Grant CHE77-16362 from the National Science Foundation. The computer time made available by the North Dakota State University Computer Center is gratefully acknowledged.

(14) Note, however, that the "aromatic character" predicted by semiempirical calculations (ref 2) for silacyclopropene is not supported by the present calculations. A similar comment has been made by Barthelat et al., ref 5.

(15) In the interest of brevity, the normal coordinates are not included here. They will, however, be made available upon request.

(16) (a) J. L. Duncan and D. C. McKean, *J. Mol. Spectrosc.*, **27**, 117 (1968); (b) T. Shimanouchi, "Tables of Molecular Vibrational Frequencies", Consolidated Vol. I, NSRDS-NBS-39, National Bureau of Standards, 1972.

(17) T. Y. Yum and D. F. Eggers, Jr., *J. Phys. Chem.*, **83**, 502 (1979).

Electronic Structure and Photoelectron Spectra of $S_2Fe_2(CO)_6$

E. L. Anderson,[1a] T. P. Fehlner,*[1a] A. E. Foti,[1b] and D. R. Salahub*[1b]

Contribution from the Department of Chemistry, University of Notre Dame, Notre Dame, Indiana 46556, and the Département de Chimie, Université de Montréal, Montréal, Québec, Canada H3C 3V1. *Received December 26, 1979*

Abstract: The valence photoelectron spectrum of $S_2Fe_2(CO)_6$ has been measured in the gas phase with Ne(I) and He(I) radiation. The observed bands are assigned on the basis of intensity changes with photon energy, relative band areas, past experience with related molecules, and molecular orbital calculations of the Extended Hückel (EH), Fenske-Hall (FH), and Self-Consistent-Field-Xα-Scattered-Wave (SCF-Xα-SW) types. While none of the theoretical approaches provides a direct quantitative interpretation of the spectrum, the overall agreement for the Xα calculations is sufficient to allow a meaningful discussion of the salient features of the binding in the series CO, $Fe(CO)_3$, $Fe_2(CO)_6$, S_2, and $S_2Fe_2(CO)_6$. The Xα results indicate *two* important Fe-Fe bonding orbitals, the HOMO of a_1 symmetry which is a slightly bent σ bonding orbital and a lower-lying b_1 orbital which has a significant direct Fe-Fe π component *induced* by interaction with the bridge. The former has previously been discussed on the basis of FH calculations but the latter has not. In addition there is a large effect of the S_2 bridge on the Fe-CO binding which shows up as a stabilization of the CO 5σ levels by nearly an electron volt compared with their position in $Fe_2(CO)_6$.

In the study of bridged binuclear transition-metal complexes a central question concerns the influence of the bridging ligands on metal-metal bonding and also on the bonding between the metal atoms and the other (terminal) ligands.[2] The question may be posed whether it is fruitful to consider $M_2T_xB_y$ (M = metal, T = terminal ligand, B = bridging ligand) as M_2T_x perturbed by the presence of the bridging ligands or as an M_2B_y fragment to which the terminal ligands are attached or, indeed, whether either of these decompositions of the molecule are of use in gaining insight into the structure, bonding, reactivity, catalytic activity, and other properties of this type of complex. Progress in several fields has allowed some first steps to be made toward answering this type of question. Two of these fields that are of direct interest to us in this paper are (i) the photoelectron spectroscopy (PES) of transition-metal complexes and (ii) molecular-orbital (MO) theory. Both PES and MO theory are currently well developed and tested tools for organic chemistry.[3] Inorganic applications,

(1) (a) University of Notre Dame. (b) Université de Montréal.

(2) (a) Teo, B. K; Hall, M. B.; Fenske, R. F.; Dahl, L. F. *Inorg. Chem.* **1975**, *14*, 3103. (b) Anderson, A. B. *Ibid.* **1976**, *15*, 2598. (c) Summerville, R. H.; Hoffmann, R. *J. Am. Chem. Soc.* **1976**, *98*, 7240. (d) Burdett, J. K. *J. Chem. Soc. Dalton Trans.* **1977**, 423. (e) Thorn, D. L.; Hoffmann, R. *Inorg. Chem.* **1978**, *17*, 126.

(3) Rabalais, J. W. "Principles of Ultraviolet Photoelectron Spectroscopy"; Wiley-Interscience: New York, 1977.

0002-7863/80/1502-7422$01.00/0

however, are at a much earlier stage of development and only in recent years has it became relatively common to obtain the PES of a transition-metal complex by using one or more light sources and also to perform MO calculations with some hope of interpreting the PES and describing the electronic structure of the molecule with a reasonable degree of confidence.[4] Advances on these two fronts now make it possible for the inorganic chemist to confront the more classical and qualitative concepts used for the description of the binding in transition-metal complexes with experimental PES results and with the results of modern electronic structure theory.

A number of theoretical approaches, each with its own set of pros and cons, are currently being advocated for calculations on transition-metal complexes. For the particular case of bridged dinuclear complexes these include traditional LCAO–Hartree–Fock and configuration interaction calculations (e.g., Bĕnard[5]), the Extended Hückel Method (e.g., Hoffmann and collaborators,[2e] Burdett[2d]), the method of Fenske and Hall[6] (e.g., Teo et al.[2a]) and calculations by the Xα method which involves a local approximation for exchange.[7] The Xα equations may be solved in a number of ways, the two most popular being the scattered-wave (SW) approach[8] (e.g., Norman et al.[9]) and the basis-set-dependent discrete variational method[10] (DV-Xα) (e.g., Heijser[11]). While each of these methods furnishes a certain amount of useful and trustworthy information, quantitative accuracy cannot yet be guaranteed for any of them and much work remains before a computationally feasible and generally applicable method of electronic structure calculation for coordination complexes is developed.

In the present paper we will be primarily concerned with the photoelectron spectra and electronic structure of the bridged diiron carbonyl $S_2Fe_2(CO)_6$. A comment concerning the significance of the d band of the ultraviolet photoelectron spectrum has previously been presented.[12] We have carried out MO calculations by using the Extended Hückel and SCF-Xα-SW methods and the results are compared below with the experimental results and also with the Fenske–Hall results of Teo et al.[2a] In addition we have made Xα-SW calculations for the molecular fragments CO, $Fe(CO)_3$, $Fe_2(CO)_6$, and S_2 in order to monitor the changes in electronic structure as one constructs the bridged carbonyl from its constituent parts. The overall picture of the metal–metal binding which emerges from the Xα calculations bears some resemblance to that inferred from the FH results; however, there are essential differences. The details of the Fe–CO binding have also been examined in some detail and we have isolated some interesting electronic effects which arise from the interactions of the two $Fe(CO)_3$ units with each other and with the S_2 bridge.

Experimental Section

The sample of $S_2Fe_2(CO)_6$ used in this work was prepared as described in the literature.[13] Mass spectrometric analysis indicated that the vapor above the solid sample at room temperature was composed of molecular $S_2Fe_2(CO)_6$. The photoelectron spectra of the vapor above the solid sample of $S_2Fe_2(CO)_6$ at room temperature were recorded by using He(I) (21.2 eV) and Ne(I) (16.8 eV) radiation. The spectrometer used has a resolution of 20 meV (fwhm) at 5 eV, and a mixture of xenon and argon was used as an internal calibrant.[14]

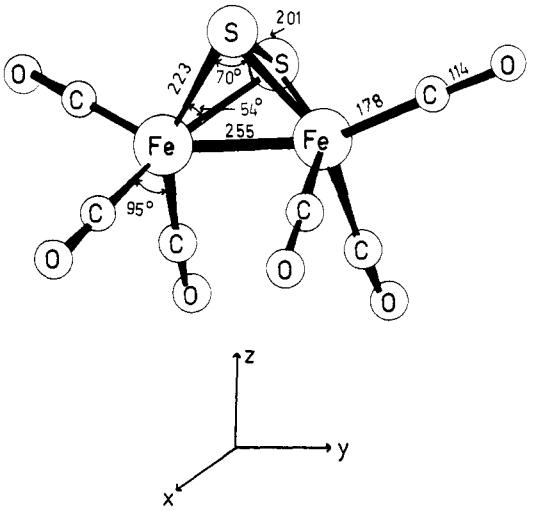

Figure 1. Geometry of $S_2Fe_2(CO)_6$. See ref 2a.

Table I. Xα-SW Computational Parameters

molecule (symmetry)	sphere sizes, bohr
CO ($C_{\infty v}$)	$R_C = 1.38, R_O = 1.38, R_{OS} = 2.50$
$Fe(CO)_3$ (C_{3v})	$R_{Fe} = 2.20, R_C = 1.38, R_O = 1.38, R_{OS} = 6.97$
$Fe_2(CO)_6$ (C_{2v})	$R_{Fe} = 2.35, R_C = 1.38, R_O = 1.38, R_{OS} = 9.14$
$S_2Fe_2(CO)_6$ (C_{2v})	$R_{Fe} = 2.35, R_S = 2.28, R_C = 1.38, R_O = 1.38, R_{OS} = 9.14$
S_2 ($D_{\infty h}$)	$R_S = 2.28, R_{OS} = 4.17$

Computational Methods and Parameters

Extended Hückel Calculations. The EH method has been described[15] and the Slater exponents and ionization potentials (eV) used in this work follow: Fe, 3d 2.600, −11.67; 4s 0.970, −9.75; 4p 0.970, −5.89. C, 2s 1.625, −21.40; 2p 1.625, −11.40. O, 2s 2.275, −32.30; 2p 2.275, −14.80. S 3s 1.820, −20.70; 3p 1.820, −11.61. The molecular geometry is the same as that used for the SCF-Xα-SW calculations described below.

Self-Consistent-Field-Xα-Scattered-Wave Calculations. The SCF-Xα-SW method has been described in detail[7,8] and several reviews of various applications exist.[16] A concise account of the salient features of the method in comparison with more traditional quantum chemical methods may be found in ref 17.

For $S_2Fe_2(CO)_6$ we have used the idealized geometry given by Teo et al.[2a] which was derived from the experimental structure[18] by averaging (slightly) different bond angles. This structure is shown in Figure 1 along with our choice of coordinate system. The same geometry was used for the $Fe_2(CO)_6$ fragment. For the $Fe(CO)_3$ fragment a tetrahedral C–Fe–C angle and an Fe–C distance of 183 pm was used as in our recent study of $B_4H_8Fe(CO)_3$.[19] This is a somewhat different geometry than that used for the bridged complexes, Fe–C = 178 pm, C(ax)–Fe–C(eq) = 98.9°, C(eq)–Fe–C(eq) = 92.2°; however, the effects of these differences on the calculated energy levels are expected to be minor. Indeed, Elian and Hoffmann[20] have performed EH cal-

(4) See, for example: Weber, J.; Geoffroy, M.; Goursot, A.; Pĕnigault, E. *J. Am. Chem. Soc.* **1978**, *100*, 3995.
(5) Bĕnard, M. *J. Am. Chem. Soc.* **1978**, *100*, 2354.
(6) Hall, M. B.; Fenske, R. F. *Inorg. Chem.* **1972**, *11*, 768.
(7) (a) Slater, J. C. *Adv. Quantum Chem.* **1972**, *6*, 1 and references therin. (b) Slater, J. C. "The Self-Consistent Field for Molecules and Solids"; McGraw-Hill: Kuala Lumpur, 1974; Vol. 4.
(8) Johnson, K. H. *Adv. Quantum Chem.* **1973**, *7*, 143 and references therin.
(9) Norman, J. G., Jr.; Kalbacher, B. J.; Jackels, S. C. *J. Chem. Soc., Chem. Commun.* **1978**, 1027.
(10) See, for example: Baerends, E. J.; Ros. P. *Int. J. Quantum. Chem.* **1978**, *S12*, 169, and references therein.
(11) Heijser, W. Ph.D. Thesis, Vrije Universiteit, Amsterdam, 1979, unpublished.
(12) Andersen, E. L.; Fehlner, T. P. *Inorg. Chem.* **1979**, *18*, 2326.
(13) Hieber, W.; Gruber, I. *Z. Anorg. Allg. Chem.* **1958**, *296*, 91.
(14) Fehlner, T. P. *Inorg. Chem.* **1975**, *14*, 934.
(15) Hoffmann, R. *J. Chem. Phys.* **1963**, *39*, 1397. Hoffmann, R.; Lipscomb, W. *Ibid.* **1962**, *36*, 3489.
(16) (a) Johnson, K. H. *Ann. Rev. Phys. Chem.* **1975**, *26*, 39. (b) Messmer, R. P. In "Modern Theoretical Chemistry", Segal, G. A., Ed.; Plenum: New York, 1977; Vol. 8. (c) Rösch, N. In "Electrons in Finite and Infinite Structures", Phariseau, P., Ed.; Plenum: New York, 1977. (d) Messmer, R. P. In "Nature of the Surface Chemical Bond", Ertl, G., and Rhodin, T. N., Eds.; North-Holland: Amsterdam, 1978.
(17) Salahub, D. R.; Foit, A. E.; Smith, V. H., Jr. *J. Am. Chem. Soc.* **1978**, *100*, 7847.
(18) Wei, C. H.; Dahl, L. F. *Inorg. Chem.* **1965**, *4*, 1; 493.
(19) Salahub, D. R. *J. Chem. Soc., Chem. Commun.* **1978**, 385.
(20) Elian, M.; Hoffmann, R. *Inorg. Chem.* **1975**, *14*, 1058.

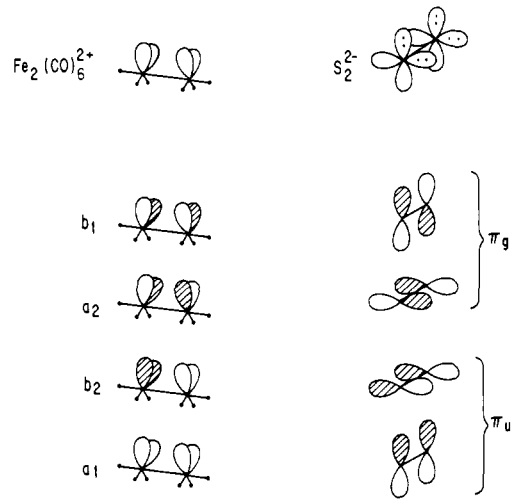

Figure 2. The fragment orbitals that interact in forming $S_2Fe_2(CO)_6$ from $Fe_2(CO)_6^{2+}$ and S_2^{2-}.

culations for an $M(CO)_3$ fragment varying the C–M–C angle from 120° (D_{3h}) to less than 90° (an octahedral fragment). Comparing their results for a tetrahedral angle and an MCM angle near 100° (θ = 109° 28′ and ≈115° in the notation of Figure 12 of ref 20), we observe that the pattern and qualitative spacing of the levels is unchanged. Hence, the tetrahedral fragment is adequate for our purposes.

We have used the overlapping sphere version of the Xα-SW method, which has been shown in a number of cases to yield improved results. The choice of sphere radii for a complicated molecule such as $S_2Fe_2(CO)_6$ which involves six independent atomic spheres in addition to the outer sphere is nontrivial. Because of the geometry, the Norman criterion[21] cannot be applied. We have settled on the ad hoc choice of sphere radii shown in Table I on the following basis. The sphere radii for C and O are those used in a previous overlapping sphere study of the CO molecule.[22] The Fe sphere radius was then chosen to yield about 30% overlap with the C sphere (defined as the ratio of the length of the overlap region to the radius of the smaller sphere) which is in line with our previous experience with overlapping spheres. It should be pointed out that with this choice of radii there is a small gap of about 6 pm between the two iron spheres. The sulfur sphere radii yield overlaps of about 40% for the S–S bond and about 20% of the Fe–S bonds. Clearly, the above choices of sphere radii are by no means unique and should be regarded simply as reasonable choices by experienced practitioners of the method. As we will see below this choice of sphere sizes appears to lead to errors in the relative positions of some of the levels, compared with the photoelectron spectrum, of the order of 1 eV. In addition to the relative errors, the calculations severely overestimate all of the ionization potentials by about 4 eV. While it is likely that fine tuning of the sphere radii could lead to improved agreement this would be a costly procedure and moreover for the purpose of obtaining a qualitative account of the binding in the molecule the present level of agreement should be sufficient. We have therefore not attempted any empirical adjustment of the radii. Tests of the effects of varying sphere radii for the simpler mononuclear carbonyls are in progress. The exchange parameters, α, were taken from the compilation of Schwarz[23] for each of the atomic spheres and averages weighted by the number of valence electrons were taken in the intersphere and outer sphere regions. In the solutions of the secular equations maximum values of the azimuthal quantum number were 1, 1, 2, and 4 for C, O, Fe, and the outer sphere, respectively. The computational parameters for CO, $Fe(CO)_3$ (point group C_{3v}), $Fe_2(CO)_6$ (C_{2v}), S_2, and $S_2Fe_2(CO)_6$ (C_{2v}) are summarized in Table I.

(21) Norman, J. G. Jr. *J. Chem. Phys.* **1974**, *61*, 4630.
(22) Salahub, D. R.; Messmer, R. P.; Johnson, K. H. *Mol. Phys.* **1976**, *31*, 529.
(23) Schwarz, K., *Phys. Rev. B.* **1972**, *5*, 2466.

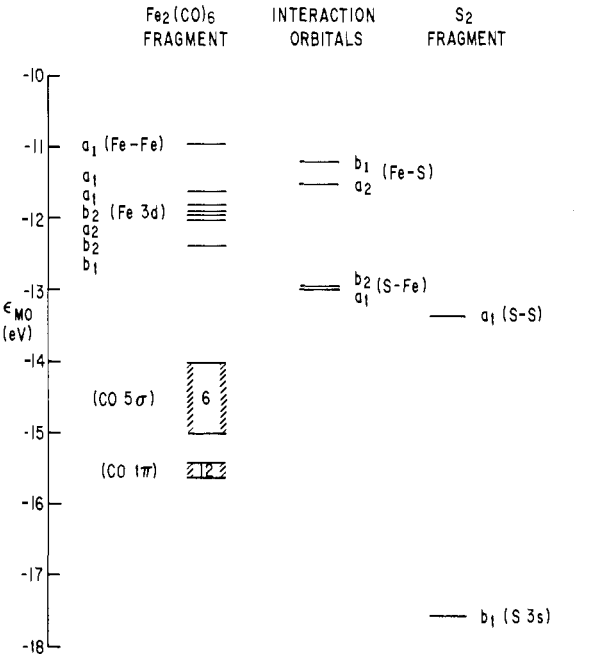

Figure 3. The filled orbital structure of $S_2Fe_2(CO)_6$ from extended Hückel calculations divided into types according to the fragment model (see text).

Table II. Vertical Ionization Potentials, Relative Band Areas, and Band Characters for $S_2Fe_2(CO)_6$

band[a]	IP,[b] eV	A/E[c] (rel)	$\frac{A/E(736\ Å)}{A/E(584\ Å)}$	IP per band (assigned)	character
1	8.2 sh				
	8.5 sh				
	8.6	1.5	0.6	7	Fe(3d)
	9.2 sh				
2	10.2	1.0	[1.0]	2	S(3p)Fe(3d)
3	12.4	1.5	0.7	3	S(3p)
4	14.2	7.7	0.6	18	CO(5σ,1π)
5	~17.5			6	CO(4σ)
6[d]	21.2			2	S(3s)
7[d]	32.5			6	CO(3σ)

[a] See Figure 4 for numbering. [b] Energies refer to band centers; sh ≡ shoulder. [c] Band area, He(I), over mean electron energy. [d] Film spectrum with Mg Kα radiation (Courtesy of Dr. S. Muralidharan).

Results and Discussion

Photoelectron Spectra. The number and type of bands in the valence region of the photoelectron spectrum of $S_2Fe_2(CO)_6$ can be understood in terms of a simple fragments-in-molecules approach.[24] In the case of the molecule of interest, one possible intuitive division is into $Fe_2(CO)_6^{2+}$ and S_2^{2-} fragements.[25] This division is not meant to imply ionic bonding but is only a device used to generate one description of the observed complete molecule. The fragment–fragment interaction orbitals can be visualized as shown in Figure 2. The $Fe_2(CO)_6^{2+}$ fragment is modeled by $Mn_2(CO)_{10}$ from which four CO ligands have been removed. The linear combinations of the resulting four empty orbitals that reflect the C_{2v} symmetry of the completed molecule are shown in Figure 2. These then have the proper symmetry to interact with the four filled π_g and π_u orbitals of the S_2^{2-} fragment. This qualitative view of the bonding in $S_2Fe_2(CO)_6$ is the same as that presented by Thorn and Hoffmann;[2e] however, in order to analyze the photoelectron spectrum all the filled orbitals must be considered, i.e., the noninteracting as well as the interacting fragment orbitals. In order to do this in a qualitative but systematic fashion, Extended

(24) See, for example: Bock, H.; Ramsey, B. G. *Angew. Chem., Int. Ed. Engl.* **1973**, *12*, 734.
(25) Photoelectron spectra of related compounds containing Fe–Fe bonds have recently been reported: Van Dam, H.; Stufkens, D. J.; Oskam, A. *Inorg. Chim. Acta.* **1978**, *31*, L377.

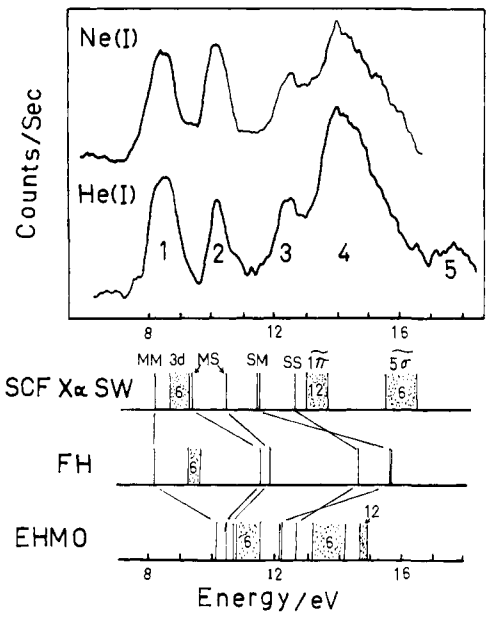

Figure 4. The UV photoelectron spectra of $S_2Fe_2(CO)_6$ and a comparison with the eigenvalues for the three computational methods. The FH results are taken from ref 2a. The Xα and EH results have been uniformly shifted (see text).

Hückel calculations were carried out on $S_2Fe_2(CO)_6$. The orbital energies as well as crude designations of orbital types are given in Figure 3. From this analysis it is clear that filled orbitals of four different qualitative types are expected: orbitals of high metal (3d) character, orbitals of metal (3d)–sulfur (3p) character, orbitals of high sulfur (3p) character, and orbitals of high CO (5σ,1π) character.

The photoelectron spectra of $S_2Fe_2(CO)_6$ are shown in Figure 4 and the data are gathered in Table II.[25] The spectra exhibit four prominent bands below 16 eV. Band positions, band intensity changes with photon energy, and past experience with the spectra of iron carbonyls[26] show that bands 1 and 4 originate in the $Fe_2(CO)_6$ fragment: peak 1 corresponding to ionizations of MO's with large Fe 3d character and peak 4 being primarily due to CO $\widetilde{5\sigma}$ and $\widetilde{1\pi}$ orbitals, where the tilda represents modifications of the free CO orbitals on complex formation. By elimination, peaks 2 and 3 result from fragment–fragment interaction orbitals, i.e., orbitals that involve the π_g and π_u orbitals of the S_2 fragment. The detailed assignment of these two peaks is problematic since, as we shall see below, the various theoretical approaches differ quite markedly as to the relative positions and detailed character of the interaction orbitals. In addition, the proximity of band 3 to band 4 leads to a rather large uncertainty in its area so that conclusions based on intensity changes with changing photon energy are somewhat tenuous. In this respect, the He(II) spectrum would be very useful, since peaks corresponding to orbitals with large sulfur 3p contributions would be expected to undergo quite dramatic intensity reductions.[27] Unfortunately, we are not presently equipped for He(II) work. With these reservations in mind, we propose the following reasonable assignment: band 1, a_1(Fe–Fe),a_1,a_1,b_1,a_2,b_2,b_2(Fe "lone pairs"); band 2, b_1,a_2(Fe–S bridge); band 3, b_2,a_1(S–Fe bridge),a_1(S–S); and band 4, CO $\widetilde{5\sigma}$ and $\widetilde{1\pi}$. The weak band (5) near 17.5 eV undoubtedly corresponds to the CO $\widetilde{4\sigma}$ levels since the He(II) spectra of a number of carbonyls show the $\widetilde{4\sigma}$ band prominently at this energy.[28] The X-ray photoelectron spectrum (Table II) reveals two bands at higher ionization potential and these are easily assigned to band 5, the symmetric and antisymmetric S 3s combinations, and band 6, CO $\widetilde{3\sigma}$.

Table III. SCF-Xα-SW Orbital Energies (eV) and Charge Distribution for $Fe_2(CO)_6S_2$

symmetry or type	$-\epsilon$	Q, % Fe	S	C^a	C^b	O^a	O^b	II^c	III^d
b_2 (LUMO)	7.6	66	8	6	5	1	2	11	0
a_1 (HOMO)	10.3	62	3	6	2	1	4	21	0
b_1	10.8	50	21	1	3	4	3	17	0
a_1	10.9	62	9	1	2	3	8	15	0
b_2	11.2	78	0	1	1	4	6	10	0
a_1	11.2	67	13	0	2	1	6	11	0
a_2	11.2	79	5	1	1	3	4	7	0
b_2	11.3	74	3	0	2	0	10	11	0
a_2	11.4	29	39	0	2	3	2	23	0
b_1	12.5	53	25	0	0	2	5	14	0
b_2	13.4	21	54	0	3	3	0	18	0
a_1	13.4	16	58	0	1	1	4	18	0
a_1	14.7	16	58	1	0	5	2	16	0
$\widetilde{1\pi}$	15.0	0	0	0	2	0	9	27	0
	−15.6	−6	−3	−13	−19	−41	−56	−29	
$\widetilde{5\sigma}$	17.5	24	0	0	5	0	1	13	0
	−18.5	−37	−2	−38	−43	−7	−12	−21	
$\widetilde{4\sigma}$	20.3	1	0	0	0	0	2	18	0
	−20.6	−3	−2	−17	−19	−60	−63	−20	−1
b_1 (S-3s)	20.4	5	80	0	0	0	1	13	0
a_1 (S-3s)	25.2	10	86	0	0	0	0	3	0

[a] Two CO groups on same side as S_2 bridge. [b] Four CO groups on opposite to S_2 bridge. [c] Intersphere charge. [d] Outer sphere charge.

Spectra vs. Calculations. In order to proceed beyond this empirical assignment one needs guidance from a theoretical model. Before doing so, however, it is useful to briefly compare the numerical results of the three theoretical techniques. This is done in Figure 4. A few preliminary comments are necessary concerning the orbital energy levels shown in Figure 4. The EH results have been uniformly shifted 0.83 eV to lower binding energy. The FH results have been taken from Figure 2 of Teo et al.;[2a] however, these authors did not report eigenvalues for the CO-derived levels. The Xα-SW results have been shifted by 2 eV to lower binding energy. We emphasize that the quantities reported are ground-state-orbital energies and not transition-state energies.[7] The transition state, in the context of Xα theory, corresponds to an artificial state in which one-half an electron is removed in a self-consistent fashion from an orbital of interest. The orbital energies for the transition state are close approximations to the calculated ionization energies of the system which otherwise would have to be computed as differences of total energies. In principle, a separate self-consistent calculation should be performed for each ionization potential; however, in practice it is often found that the energy shifts involved are nearly constant. We have verified this for the present case by performing transition-state calculations for three levels, the HOMO which is metal–metal bonding, the uppermost occupied a_2 level which is metal nonbonding, and the second uppermost a_2 level which has large contributions from both Fe and S orbitals. For these three levels which correspond to quite different electronic arrangements the transition-state shifts are 2.1, 2.3, and 2.1 eV, respectively, so that differential relaxation appears to be small. With this transition state shift the absolute discrepency between the calculated first IP and the experimental value is about 4 eV. This rather large absolute error is probably due in the main to the geometry of the molecule and the consequent difficulty in the choice of the sphere radii.

Examining the results of the three computational methods shown in Figure 4 one can identify both similarities and differences. In order to facilitate the discussion, we show in Table III the calculated Xα charge distributions for the various orbitals. We

(26) Ulman, J. A.; Anderson, E. L.; Fehlner, T. P. *J. Am. Chem. Soc.* **1978**, *100*, 456.

(27) The 3p ionization cross-section for atomic sulfur passes through a "Copper minimum" for an electron kinetic energy near 35 eV. The dramatic decrease in cross-section compared with lower kinetic energies is also present for the three valence levels of H_2S which involve S 3p (see Roche, M.; Salahub, D. R.; Messmer, R. P. *J. Electron Spectrosc. Relat. Phenom.* **1980**, *19*, 273). Similar effects have been observed, for example, in the case of Cl 3p levels in $Rh_2Cl_2(CO)_4$ (Nixon, J. F.; Suffolk, R. J.; Taylor, M. J.; Norman, J. G., Jr.; Hoskins, D. E.; Gmur, D. J. *Inorg. Chem.* **1980**, *19*, 810).

(28) Plummer, E. W.; Salaneck, W. R.; Miller, J. S. *Phys. Rev. B* **1978**, 1673.

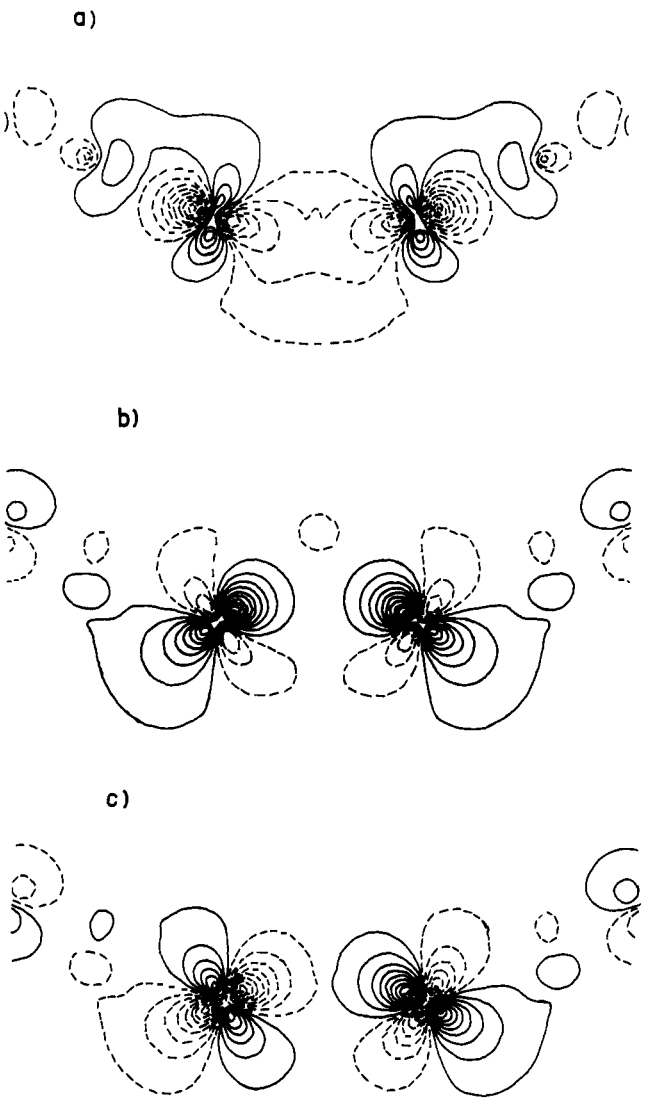

Figure 5. Contour plots of selected molecular orbital wave functions of $S_2Fe_2(CO)_6$ in the *yz* plane (see Figure 1): (a) the a_1 (HOMO) level at −10.3 eV; (b) the a_1 level at −10.9 eV; (c) the b_2 level at −11.2 eV. The lowest contour has the value (a) 0.0328, (b) 0.0327, (c) 0.0356 au, and adjacent contours differ by (a) 0.0642, (b) 0.0642, (c) 0.0697 au.

see that the occupied orbitals with a large charge on the iron atoms (≥50%) may be separated into three groups, namely, the HOMO of symmetry a_1 (ϵ = −10.3 eV), six close-lying levels in the orbital energy region −10.8 to −11.3 eV, and the b_1 level at −12.5 eV. While there is some admixture in these levels from the sulfur and the CO groups, they are clearly predominantly metal orbitals. Those of b_1 symmetry (10.8 eV and 12.5 eV) also have significant contributions from the sulfur and are discussed in more detail below. All three methods agree on the qualitative nature and rough ordering of these levels. The HOMO is an Fe–Fe bonding orbital which shows some bending away from the S_2 bridge. A contour plot of the Xα wave function for this level is shown in Figure 5a which is very similar to the FH wave function shown in Figure 3 of ref 2a. The HOMO is followed in the Xα and FH calculations by an energy gap and then six levels which are primarily bonding and antibonding combinations of iron d functions which are quite contracted leading to small overlaps and a narrow band of levels. Contour plots for two of these levels, one formally bonding the other formally antibonding, are shown in Figure 5b in order to illustrate the localized atomic nature of the wave functions. The EH method also gives the same pattern; however, some of the sulfur levels also appear in this energy region. From a quantitative point of view the principal difference among the results of the different calculations for this upper group of levels is in the magnitude of the gap between the HOMO and the "lone pair" levels which is predicted to be about 0.5 eV by Xα, about 1 eV by FH, and about 0.6 eV by EH. The profile of the first experimental PES band favors the smaller values.[12]

The next set of energy levels and photoelectron peaks 2 and 3 involve the bridging S_2 group and here the three theoretical approaches diverge seriously as regards the spacing between the sulfur-derived levels, their energy juxtaposition with respect to the metal levels, and, as we shall see below, their intrinsic character. None of the methods results in a quantitative assignment of peaks 2 and 3. Peak 4 of the PES is certainly due to the CO $1\tilde{\pi}$ and $5\tilde{\sigma}$ ionizations and the Xα calculations put these two bands near the correct relative energy with the $1\tilde{\pi}$ bands preceding the $5\tilde{\sigma}$ and a significant gap between the two which will be discussed in more detail below. The EH method places these levels at lower binding energy and inverts their order, giving the $5\tilde{\sigma}$ as less tightly bound than the $1\tilde{\pi}$. The relative stability of the $5\tilde{\sigma}$ levels with respect to the $1\tilde{\pi}$ is important to the following discussion and so deserves some comment. The Xα calculations predict a gap of 1.7 eV between the deepest $1\tilde{\pi}$ level and the uppermost $5\tilde{\sigma}$ level. A similar gap of 2 eV was found by Nixon et al.[27] in an Xα calculation of $Rh_2Cl_2(CO)_4$ which is like $S_2Fe_2(CO)_6$ in that it involves an electronegative bridge. The ($1\tilde{\pi}$, $5\tilde{\sigma}$) peak in the He(II) spectrum of $Rh_2Cl_2(CO)_4$ shows a definite shoulder at 15.0 eV followed by a peak at 16.08 eV which have been assigned to $1\tilde{\pi}$ and $5\tilde{\sigma}$ ionizations, respectively. In the case of $S_2Fe_2(CO)_6$ (peak 4 of Figure 4) the two bands are not resolved. While the overall width of peak 4 (~3 eV) is reasonably consistent with the calculations, any straightforward decomposition of the band profile into (vibrationally broadened) peaks centered at the calculated energies would indicate that the separation of the two groups of levels is overestimated in the calculations. A similar conclusion may be reached for the $Rh_2Cl_2(CO)_4$ calculations of ref 27. Notwithstanding these quantitative imperfections of the calculations we give below a detailed qualitative description of the interactions among the various moieties of $S_2Fe_2(CO)_6$ based on the Xα calculations. While we believe the overall description is valid, the reader is now aware that the relative positions of the energy levels may be in error by an eV or so and that hence the effects discussed below may be somewhat overestimated or underestimated. The total picture of the binding and interactions in $S_2Fe_2(CO)_6$ which emerges from the calculations is coherent and appealing and we believe the present calculations will serve as a good basis for future theoretical and experimental work aimed at refining the quantitative aspects.

Analysis of Bonding. We now wish to discuss in some detail the binding in $S_2Fe_2(CO)_6$ based on the Xα orbital energies and wave functions for the complex and its constituent parts, CO, $Fe(CO)_3$, $Fe_2(CO)_6$, and S_2. Somewhat similar analyses have previously been presented for $S_2Fe_2(CO)_6$ based on the Fenske–Hall calculations[2a] and for some related bridged $Fe_2(CO)_6X_2$ complexes based on the Extended Hückel method.[2e] The following discussion is to some extent confirmatory of these works; however, the detailed interpretation of the Fe–Fe and Fe–S–Fe binding which emerges from the Xα study differs in some essential features. In addition, the perturbation of the Fe–CO binding by the S_2 bridge has some interesting aspects.

The calculated Xα orbital energies for CO, $Fe(CO)_3$, $Fe_2(CO)_6$, $S_2Fe_2(CO)_6$, and S_2 are shown in Figure 6. The CO results are from ref 22, and these and similar results are discussed in the literature. Complexing three CO groups with an iron atom produces the energy level scheme shown in part b of Figure 6. The calculated charge distribution is given in Table IV. The uppermost occupied levels are highly concentrated on the metal and are essentially those discussed in detail by Elian and Hoffmann[20] based on EH calculations and we have nothing essential to add to their discussion. The lower part of the spectrum involves orbitals which are readily identifiable with the valence orbitals of CO modified somewhat by interactions with the Fe. As is well known the major effect of complexing the CO occurs for the $5\tilde{\sigma}$ level which is stabilized by about 3 eV.[29] Our calculations indicate

(29) Johnson, J. B.; Klemperer, W. G. *J. Am. Chem. Soc.* **1977**, *99*, 7132.

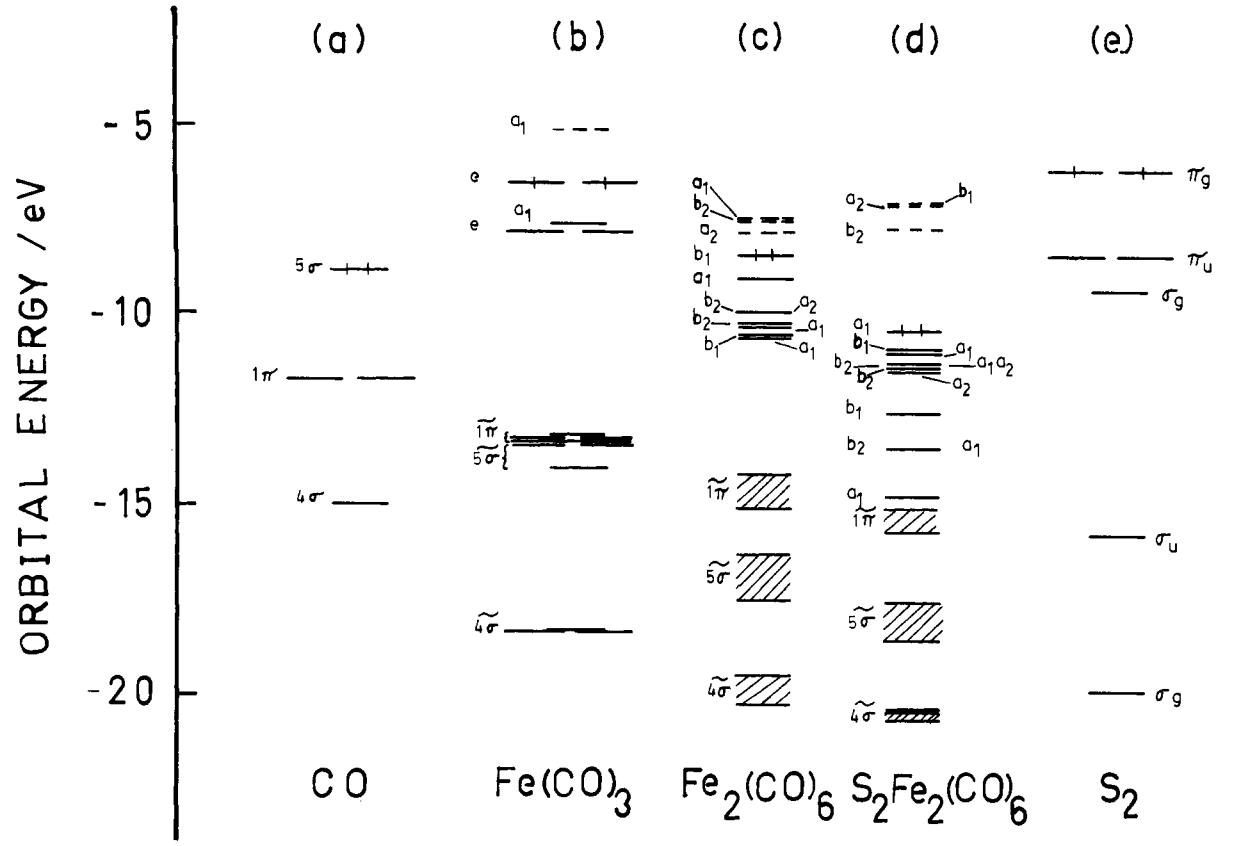

Figure 6. SCF-Xα-SW orbital eigenvalues (eV) for (a) CO, (b) $Fe(CO)_3$, (c) $Fe_2(CO)_6$, (d) $S_2Fe_2(CO)_6$, (e) S_2.

Table IV. SCF-Xα-SW Orbital Energies (eV) and Charge Distributions for $Fe(CO)_3$

		Q, %				
symmetry or type	$-\epsilon$	Fe	C	O	II[a]	III[b]
a_1 (LUMO)	5.0	7	13	10	66	4
e (HOMO, $2e^-$)	6.4	59	9	6	26	0
a_1	7.5	79	2	3	15	0
e	7.7	78	2	6	13	0
$\widetilde{1\pi}$	13.1	0	15	52	27	0
	-13.3	-2	-17	-57	-29	
$\widetilde{5\sigma}$	13.3	18	44	6	24	0
	-13.9	-24	-46		-32	
$\widetilde{4\sigma}$	18.2	0	15	67	15	2
				-68		-3

[a] Intersphere charge. [b] Outer sphere charge.

Table V. SCF-Xα-SW Orbital Energies (eV) and Charge Distributions for $Fe_2(CO)_6$ (C_{2v})

		Q, %						
symmetry or type	$-\epsilon$	Fe	C[a]	C[b]	O[a]	O[b]	II[c]	III[d]
a_1	7.3	23	3	10	3	7	53	0
b_2	7.4	67	4	6	2	3	18	0
a_2 (LUMO)	7.7	70	1	9	1	3	16	0
b_1 (HOMO)	8.3	62	1	6	2	3	25	0
a_1	8.9	61	5	4	1	6	23	0
b_2	9.8	77	1	2	4	5	10	0
a_2	9.8	80	1	1	5	4	9	0
b_2	10.1	78	0	3	0	8	10	0
a_1	10.2	77	0	3	0	9	11	0
b_1	10.4	78	0	1	4	5	11	0
a_1	10.5	81	0	1	4	3	11	0
$\widetilde{1\pi}$	14.1	0	0	0	0	2	26	0
	-15.0	-3	-16	-19	-52	-57	-28	
$\widetilde{5\sigma}$	16.2	25	0	0	0	0	14	0
	-17.4	-35	-42	-47	-12	-6	-22	
$\widetilde{4\sigma}$	19.4	1	0	0	0	0	17	0
	-20.2	-2	-17	-17	-64	-66	-19	-1

[a] Two CO groups on same side as (missing) S_2 bridge. [b] Four CO groups on opposite side to (missing) S_2 bridge. [c] Intersphere charge. [d] Outer sphere charge.

that this stabilization is just large enough for the case of $Fe(CO)_3$ to bring the $\widetilde{5\sigma}$ levels into the same energy range, and slightly below the relatively unperturbed $\widetilde{1\pi}$ levels. This situation is by now quite familiar, in particular from studies of CO chemisorption by angle-resolved photoelectron spectroscopy, and for the case of CO in Ni the inversion of the $\widetilde{5\sigma}$ and $\widetilde{1\pi}$ levels has been proved.[30]

If one brings two $Fe(CO)_3$ groups together in the geometry eventually found in $S_2Fe_2(CO)_6$ then the energy levels shown in Figure 6c result. The charge distribution is shown in Table V. Our calculation confirms the orbital ordering and rough spacings of the levels found by Thorn and Hoffmann[2e] (see Figure 2 of ref 2e). The picture of the metal–metal bond that emerges is that of a formal double bond involving the HOMO of b_1 symmetry and the next highest occupied a_1 orbital. These are followed by six tightly nested levels which are formally bonding and antibonding combinations of metal d functions on the two centers for which the overlap is very small and they are thus best regarded as nonbonding. In Figure 7a,b we show contour plots of the b_1 (HOMO) and a_1 levels in the *xy* plane. The a_1 level clearly corresponds closely to a σ bond directed along the Fe–Fe axis. The b_1 level is more complicated and since it is crucial to the ensuing discussion we describe it in some detail. Under C_{2v} the b_1 representation contains bonding combinations of both $d_{xy}(\pi)$ and $d_{xz}(\delta)$ functions (see axis choice in Figure 1) on the two irons. As far as the iron contribution is concerned the HOMO of $Fe_2(CO)_6$ is a δ–π hybrid which Thorn and Hoffmann represent as:

(1)

(30) Allyn, C. L.; Gustafsson, T.; Plummer, E. W. *Solid State Commun.* **1978**, *28*, 85.

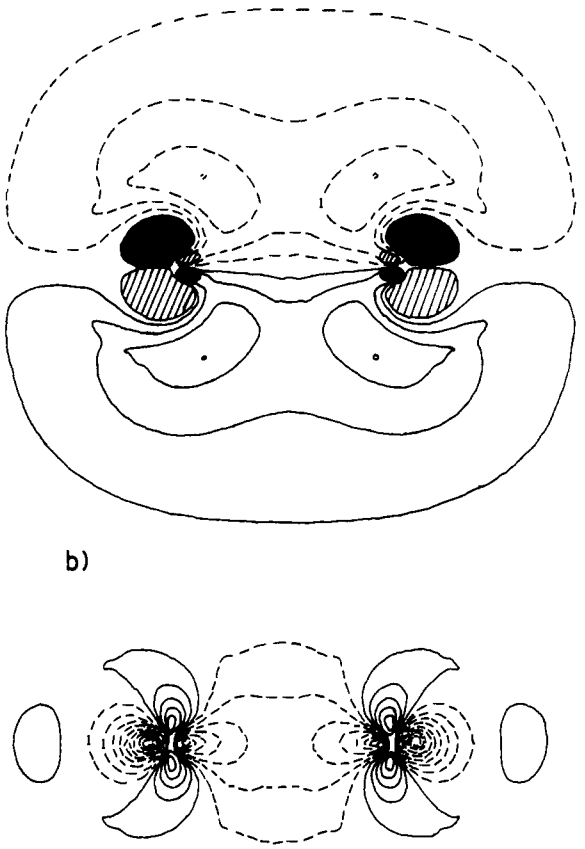

Figure 7. Contour plots of selected molecular orbital wave functions of $Fe_2(CO)_6$ (C_{2v}) in the xy plane (see Figure 1): (a) the b_1 (HOMO) level at −8.3 eV, (b) the a_1 level at −8.9 eV. The lowest contour has the value (a) 0.0079 and (b) 0.0268 au, and adjacent contours differ by (a) 0.0156 and (b) 0.0526 au.

Clearly the essence of this orbital cannot be shown in a single contour plot. The section shown in Figure 7a in fact resembles a p–d hybrid (the orbital contains 13% p character and 87% d) and we leave it to the reader to construct the rest of the three-dimensional orbital shown in **1**. It is important to point out that the amplitude of the wave function in this plane is rather small. The maximum contour in the outer lobes is 0.047 au. Our reasons for showing this particular cut and for citing the amplitude will become clear below. Note that the HOMO–LUMO gap for $Fe_2(CO)_6$ is very small (0.3 eV), consistent with the presumed reactivity of the fragment and its propensity to accept further ligands.

The formation of the $Fe(CO)_3$ dimer has also had a significant effect on the CO levels, namely a net stabilization of the $5\tilde{\sigma}$ levels with respect to the $1\tilde{\pi}$ by about 1 eV. Presumably this arises since the metal–metal bonding orbitals withdraw electron density from the region near the iron nuclei and this can be compensated in an energetically favorable manner by further donation from the $5\tilde{\sigma}$ levels. Thus, all other things being equal, one would expect stronger Fe–CO bonds for the dimer compared with the monomer.

The final step in the formation of $S_2Fe_2(CO)_6$ involves interaction of $Fe_2(CO)_6$ with an S_2 molecule to form the bridge. The energy levels for S_2 at the S–S distance of 201 pm found in the complex are shown in Figure 6e. The most important orbital for the formation of the complex is the π_g level which in isolated S_2 is partially occupied by two electrons. Under C_{2v} symmetry this orbital splits into a b_1 component involving functions parallel to the C_2 axis (p_z in our coordinate choice) and an a_2 component involving p_y functions. In the discussion of Teo et al.[2a] these orbitals were given a somewhat secondary importance as far as the Fe–Fe bonding was concerned. In contrast to this, the Xα calculations indicate that the b_1 level involves an essential metal–metal interaction. We find quite strong covalent mixing throughout the b_1 manifold. Three orbitals are involved, the two b_1 levels of $Fe_2(CO)_6$ and the b_1 component of the π_g orbital of

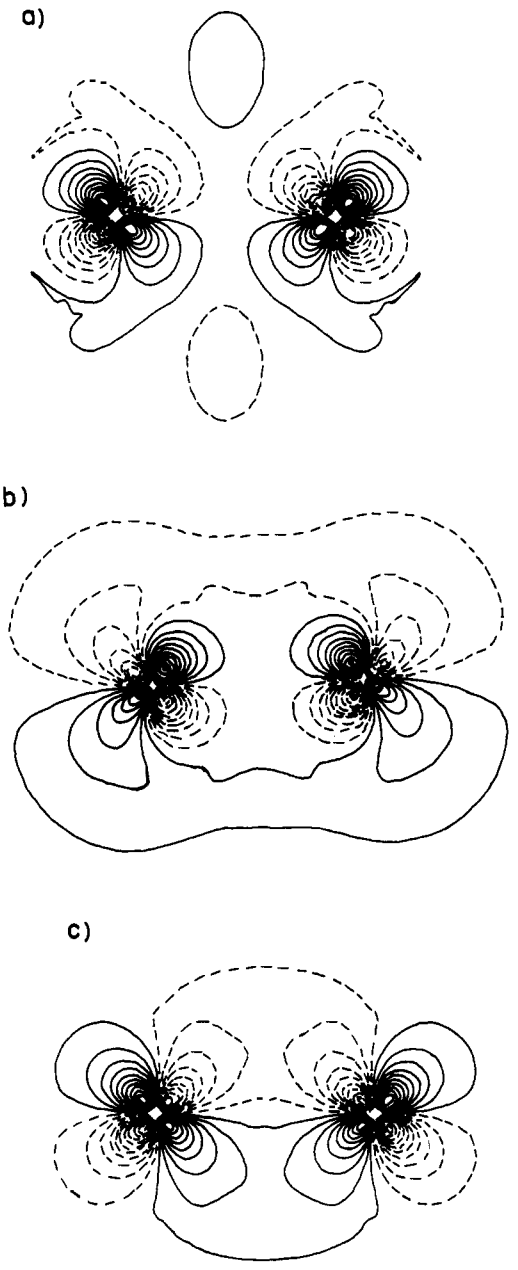

Figure 8. Contour plots of selected molecular orbital wave functions of $S_2Fe_2(CO)_6$ in the xy plane (see Figure 1): (a) the virtual b_1 level at −7.0 eV, (b) the b_1 level at −10.8 eV, (c) the b_1 level at −12.5 eV. The lowest contour has the value (a) 0.0122, (b) 0.0160, (c) 0.0225 au, and adjacent contours differ by (a) 0.0240, (b) 0.0314, (c) 0.0442 au.

S_2. In $S_2Fe_2(CO)_6$ these yield two occupied and one virtual b_1 levels and all of these receive large contributions from both iron and sulfur. Contour plots are given in Figure 8a–c in the xy plane in order to illustrate the degree of Fe–Fe bonding in each. With respect to interactions between the Fe d functions and the S_2 π_g function, which may readily be imagined in the plane perpendicular to that shown, the three orbitals are antibonding, roughly nonbonding (approximate cancellation of bonding and antibonding contributions consistent with the small change in the energy compared with the corresponding level of $Fe_2(CO)_6$), and bonding, respectively. The lowest of these levels (Figure 8c), far from being mainly $S_2(\pi_g)$, has about twice as much charge in the iron spheres as in the sulfur spheres, i.e., the contribution from the b_1 HOMO of $Fe_2(CO)_6$ is larger than that of $S_2(\pi_g)$. Comparison of Figures 7a and 8c reveals that the S_2 bridge has provoked a rehybridization of the b_1 Fe–Fe orbital. Whereas in $Fe_2(CO)_6$ this was a δ–π hybrid directed out of the plane with a rather small maximum amplitude (0.047 au) in the xy plane, for $S_2Fe_2(CO)_6$ the π component is dramatically enhanced so that Figure 8c has the

appearance of a typical metal-metal π bond. For comparison, the maximum in-plane amplitude is 0.442 au. Thus the presence of the S_2 bridge has enhanced the π component of the metal-metal bond and moreover has significantly stabilized the level. Since π bonding is typically stronger than δ bonding it appears that the S_2 unit not only serves as a bridge so that Fe-S-Fe binding may occur but in fact also allows an increase in the *direct* (through space) Fe-Fe interaction. The stabilization of the b_1 level is one of the leading factors for the increased HOMO-LUMO gap in the bridged complex and its consequent stability. In summary, rather than a single metal-metal bonding orbital, $S_2Fe_2(CO)_6$ possesses, according to the Xα calculations, some multiple Fe-Fe bond character arising from bent, nearly σ bonding in the HOMO and a significant direct π component in the b_1 orbital at -12.5 eV. It is interesting to note in this regard that SCF-Xα-SW calculations on $Fe_2S_2(SH)_4^{2-}$ show that the major Fe-Fe bonding interaction occurs via the bridging sulfurs.[9]

It may be of some interest to note that the orbital ordering in $Fe_2(CO)_6$ is reminiscent of what Hoffmann and collaborators[31] have termed counterintuitive orbital mixing, (COM), that is the two Fe-Fe bonding levels, b_1 and a_1, are less stable than the group of nonbonding levels owing to appropriate small admixtures of CO character into the wave functions. The addition of the S_2 bridge removes one of the cases of COM by stabilizing the b_1 level so that in $S_2Fe_2(CO)_6$ it is below the nonbonding orbitals. The a_1 level, however, remains "counterintuitive".

The CO levels are also influenced by the addition of the S_2 bridge, the major effect being a further stabilization of the $\widetilde{5\sigma}$ levels by about 0.7 eV compared to their position relative to $\widetilde{1\pi}$ in the $Fe_2(CO)_6$ fragment; so once again, all other things being equal, one might expect a stronger Fe-CO bond in $S_2Fe_2(CO)_6$ than in $Fe_2(CO)_6$. Again, the reason is likely that the addition of the bridging S_2 unit causes a migration of electrons away from the Fe nuclei allowing further σ donation from the carbonyls. It is our hope that once calculations are at hand for a sufficient number of transition-metal carbonyls and for cluster models of CO adsorbed on different transition metals one might be able to correlate the position of the $\widetilde{5\sigma}$ levels with the catalytic activity of the different systems for reactions involving CO (e.g., the Fischer-Tropsch synthesis of hydrocarbons). Work in this direction is in progress.

Acknowledgment. D.R.S. is grateful to the Natural Sciences and Engineering Research Council of Canada and to the Research Corporation for support of this work. T.P.F. acknowledges the support of the National Science Foundation (CHE 79-15220). In addition we wish to thank Professor Roger DeKock, Calvin College, Grand Rapids, MI for performing the Hückel calculations and Dr. S. Muralidharan for the Mg Kα spectrum of $S_2Fe(CO)_6$.

(31) Whangbo, M. H.; Hoffmann, R., *J. Chem. Phys.* **1978**, *68*, 5498.

The Proton in Dimethyl Sulfoxide and Acetone. Results from Gas-Phase Ion Equilibria Involving $(Me_2SO)_nH^+$ and $(Me_2CO)_nH^+$

Y. K. Lau, P. P. S. Saluja, and P. Kebarle*

Contribution from the Chemistry Department, University of Alberta, Edmonton, Canada T6G 2G2. *Received May 13, 1980*

Abstract: The gas-phase equilibria $(Sl)_{n-1}H^+ + Sl = (Sl)_nH^+$, where Sl are the solvent molecules dimethyl sulfoxide and acetone, were measured with a pulsed electron beam high ion source pressure mass spectrometer. $\Delta H_{n-1,n}^\circ$ and $\Delta S_{n-1,n}^\circ$ were obtained for $n = 1$ to $n = 3$. These results are compared with previously determined values for Sl = H_2O, Me_2O, and MeCN and literature data for the transfer of the proton from the gas phase to the liquid solvent $\Delta H_{tr}(H^+)^{g\rightarrow Sl}$. The highly exothermic transfer enthalpy for Me_2SO is a result of the strong interactions from $n = 1$ to $n = 3$, particularly $n = 1$, i.e., the high proton affinity of Me_2SO. Interactions for $(Me_2SO)_nH^+$ for higher n must be considerably weaker than those for $(H_2O)_nH^+$.

Introduction

The present work is part of a continuing effort from this laboratory to provide additional insights on ion solvation by means of measured binding energies between the ion and a limited number of solvent molecules.[1-3] The energies are obtained by determining gas-phase ion equilibria $(n-1,n)$ involving a given positive or negative ion $M^\pm$ and solvent molecules Sl.

$$(n-1,n) \qquad M^\pm(Sl)_{n-1} + Sl = M^\pm(Sl)_n$$

Dimethyl sulfoxide, Me_2SO, is probably the most important dipolar aprotic solvent.[4] Following earlier measurements involving another dipolar aprotic solvent, acetonitrile, a program of measurements was undertaken involving Me_2SO with the alkali positive ions and halide negative ions,[5] large delocalized organic anions,[6] and the proton (present work). Regarding the proton, it was thought of interest to compare the Me_2SO results with those for some other dipolar aprotic solvents. Fortunately Meot-Ner[7] has published recently a study involving acetonitrile. We chose to do also acetone, which bears some structural similarity to dimethyl sulfoxide but is a much weaker dipolar solvent. This makes a comparison of these three solvents possible.

Experimental Section

The equilibrium constant $K_{n-1,n}$ for the reaction

$$H^+(Me_2SO)_{n-1} + Me_2SO = H^+(Me_2SO)_n$$

was obtained from the expression

$$K_{n-1,n} = \frac{I_n}{I_{n-1}} \frac{1}{P_{Me_2SO}}$$

(1) Kebarle, P. *Annu. Rev. Phys. Chem.* **1977**, *28*, 445.
(2) Kebarle, P.; Davidson, W. R.; French, M.; Cumming, J. B.; McMahon, T. B. *Discuss. Faraday Soc.* **1978**, *64*, 220.
(3) Kebarle, P. In "Modern Aspects of Electrochemistry"; Conway, B. E., Bockris, J. O'M., Eds.; Plenum Press: New York, 1974; Vol. 9, p 1. Kebarle, P. In "Ions and Ion Pairs in Organic Reactions"; Szwarc, M., Ed.; Wiley-Interscience, New York, 1972.
(4) Jacob, S. W., Rosenbaum, E. E., Wood, D. C., Eds. "Dimethyl Sulfoxide"; Marcel Dekker: New York, 1971.
(5) Magnera, T. B.; Sunner J.; Kebarle, P., to be submitted for publication.
(6) Magnera, T. B.; Kebarle, P., to be submitted for publication.
(7) Meot-Ner, M. *J. Am. Chem. Soc.* **1978**, *100*, 4694.

0002-7863/80/1502-7429$01.00/0